Infrared nano-imaging and -spectroscopy of N graphene layers on SiO_2 and hexagonal boron nitride substrates.

Ingrid D. Barcelos,[1*] Alisson R. Cadore,[2] Leonardo C. Campos,[2] K. Watanabe,[3] T. Taniguchi,[3] F. C. B. Maia,[3] Raul Freitas,[1] Ângelo Malachias,[2] Christoph Deneke[4,5]

[1]Laboratório Nacional de Luz Síncrotron (LNLS/CNPEM), Rua Giuseppe Máximo Scolfaro 10000, 13083-100, Campinas, São Paulo, Brasil
[2]Departamento de Física, Universidade Federal de Minas Gerais, 30123-970 - Belo Horizonte, Minas Gerais, Brasil
[3]Advanced Materials Laboratory, National Institute for Materials Science, 1-1 Namiki, 305-0044 - Tsukuba, Japan
[4]Laboratório Nacional de Nanotecnologia (LNNano/CNPEM), Rua Giuseppe Máximo Scolfaro 10000, 13083-100, Campinas, São Paulo, Brasil
[5]Departamento de Física Aplicada, Instituto de Física "Gleb Wataghin", Universidade Estadual de Campinas, 13083-859 - Campinas, São Paulo, Brasil.

*ingrid.barcelos@lnls.br

Keywords: *graphene plasmons, boron nitride, phonons polaritons*

Abstract

The optical response of exfoliated graphene on different surfaces (silicon dioxide (SiO_2) and hexagonal boron nitride (hBN)) is investigated via scattering-type scanning near-field optical microscopy (s-SNOM) using broadband infrared synchrotron radiation. Basically, we use a commercial s-SNOM microscope integrated into the infrared synchrotron-based beamline to investigate with nanoscale resolution the optical response of different graphene layers on SiO_2 or hBN substrates. Comparing atomic force microscopic topography and broadband mid-infrared images (lateral resolution of 30 nm), we confirm that optical response of both systems depends on the specific interactions between graphene and substrate as well as on the number of graphene layers. This dependence is explained by particular interactions of graphene and SiO_2, wherein graphene plasmons couple to surface phonon-polaritons of SiO_2. In the case of graphene and hBN, we observe coupling of the graphene plasmon to the hyperbolic phonon-polaritons of hBN.

Introduction

Two-dimensional (2D) materials, for which graphene is the archetype of such material classes, have obtained tremendous attention in the last decade. They are regarded as future building blocks for advanced electrical or optoelectrical devices with a large variety interesting properties.[1,2] Especially for photonics and optoelectronics applications, graphene is a promising material due to its strong interaction with light.[3–5] For basic properties understanding and further integration into currently used device structures, a detailed characterization on the nanometer scale is required. In this context, scattering-type scanning near-field optical microscopy (s-SNOM) has been established as a powerful tool for these systems and provides new insights for understanding the properties and characterization of 2D materials at the nanometer scale.[6–8] Using a single wavelength line or tunable laser integrated to special optical setups, plasmons and polaritons coupling to the underlying substrates were observed and directly imaged.[9–13] Additionally, broadband infrared (IR) imaging and synchrotron infrared nanospectroscopy (SINS),[14–16] have also opened the opportunity to optically characterize 2D systems at the nanometer scale.

In this work, we use a s-SNOM setup installed in a synchrotron-based mid-IR endstation to investigate the optical response of graphene transferred to a SiO_2 as well as to a hexagonal boron nitride (BN) surface. We study the optical mid-IR scattering response of the transferred graphene flakes which depends on the number of graphene layers, as well as on the surface below the graphene. Our broadband IR s-SNOM images show clear contrast between the G/hBN and the G/SiO_2, and we observe a non-linearity in the single strength as the function of the number of layers. Furthermore, we clearly see an influence of the optical properties of the graphene due to the choice of the underlying substrate. To understand the nature of the interaction between the graphene layer and the substrates, we carried out SINS measurements, setting a spatial resolution of 100 nm. The obtained SINS spectra demonstrate the coupling between surface plasmons

DOI: 10.17648/bwsp-2017-79325

of graphene and phonons of SiO_2 and also the coupling between surface plasmons of graphene and hyperbolic phonon polaritons of hBN, in agreement with recent works.[4,6,7,17,18]

Methods and Results

Experiments were carried out on the IR nanospectroscopy beamline of the Brazilian Synchrotron Light Laboratory (LNLS, Campinas).[19,20] In this beamline, the synchrotron light is collimated and then coupled into a commercial s-SNOM microscope (Neaspec GmbH).[15] The commercial instrument is basically an atomic force microscope (AFM) equipped with an external optics which is able to focus the incident light, in this case the synchrotron beam, onto a metallic AFM tip. The tip shaft acts as an elongated antenna, which enhances the incident electrical field at the apex of the tip. The result is the generation of a near-field IR broadband light source with the size of the tip apex and wavelength independent. For IR broadband imaging, we follow the typical s-SNOM setup as layout in literature.[21] Instead the single wavelength laser we use the synchrotron beam as light source, hence obtaining an optical image constructed from the response in the whole sensitivity range of the MCT detector. The obtained optical signal is modulated by the frequency of the AFM tip (ca. 300 kHz) and the optical signal is demodulated at the 2nd harmonic of the tip frequency. As the setup uses a lock-in amplifier for the detection, amplitude and phase of the optical signal are measured simultaneously with the AFM topography map. For the acquisition of SINS spectra, the microscope is mounted after a Michelson interferometer. We obtained 20 SINS spectra per point in our measurements, which are averaged to improve the signal to noise ratio and normalized to spectra acquired from a pure Au surface.

Exfoliated graphene flakes attained by standard scotch tape method were transferred to silicon wafers with a 300 nm thick top SiO_2 layer or on top of hBN flakes previously deposited on a similar Si/SiO_2 substrate. The fabrication of graphene on hBN substrates were achieved as described in the literature.[22,23] All flakes were initially submitted to thermal annealing at 350° C with constant flow of Ar/H_2 (300:700 sccm) for 3.5 h, in order to remove any residue reminiscent from the transfer process. The graphene flakes were pre-characterized by optical light microscopy as well as post-characterized by Raman scattering to determine the number of graphene layers.[24]

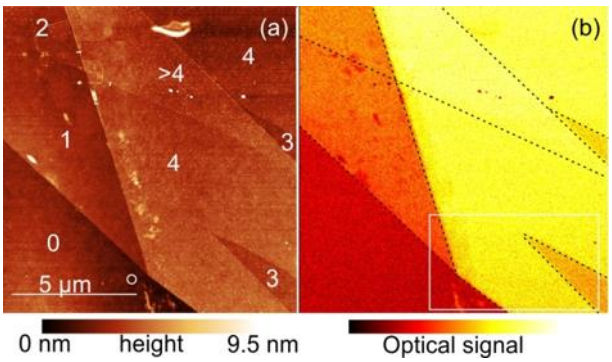

Figure 1: (a) AFM overview topography image of the graphene flake on a SiO_2 surface. The numbers of graphene layers (1 to 4) are marked in the image. The white circle in the 0 layer region marks the position of the SiO_2 reference spectrum. (b) Optical near-field image of the same region obtained using the broadband light. Black dashed lines mark the edges of different layer as seen in the AFM image. The white square box marks the inset in Fig. 3(a).

Fig. 1(a) shows the AFM topography obtained from on G/SiO_2 sample. The height contrast allows us to identify different areas with a varying number of graphene layers ranging from 1 to more than 4 layers. The exact number of graphene layers were deduced from Raman spectra. Furthermore, we marked by a white circle the position, where the reference spectra of the SiO_2 substrate were measured. Fig. 1(b) shows the optical near-field image of the same region acquired simultaneously with the AFM image of Fig. 1(a). For further clarity, we marked the different areas of the graphene sheets inside the optical image. We observe a clear optical broadband response from the graphene layer as thin as a monolayer. The optical signal is homogeneous for a specific number of layers (only areas where we can identify dirty or layer defects in AFM show a lower optical signal) and the signal strength varies for different number of layers, allowing the direct determination of the thickness for small amounts of piled layers. Interestingly, the optical response does not scale linearly with the number of layers. We cannot distinguish 1 and 2 layers of graphene in the optical image and 4 and more layers also show a similar optical response.

In Fig. 2(a), we depict the AFM topography of a graphene flake transferred to an hBN flake of 25 nm height lying on a Si/SiO_2 substrate. Again, we can identify the different numbers in the graphene layer by the height contrast. The exact number marked in the image was deduced from Raman spectra after the measurements. Fig. 2(b) shows optical near-field signal acquired simultaneously with the AFM image of Fig. 2(a). A clear optical response was observed from the hBN substrate as well as from the graphene layers. Again, we can identify the different numbers

DOI: 10.17648/bwsp-2017-79325

of layers by the strength of the optical contrast. Similarly, as shown for graphene/SiO_2, graphene onto hBN appears with a homogeneous contrast for certain number of layers but with different intensity. Only larger defects at the edges of the graphene layers result in a smaller optical signal.

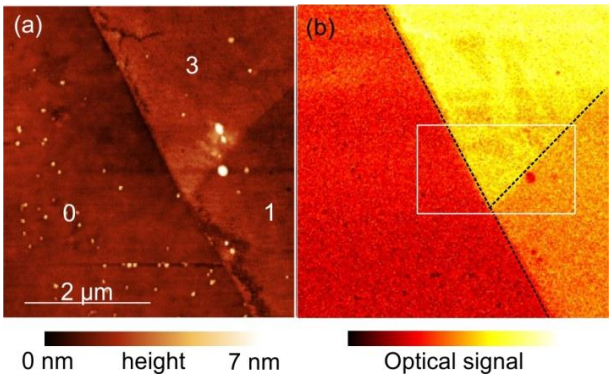

Figure 2: (a) AFM topography overview image of a graphene flake transferred to a hBN flake lying on a Si/SiO_2 substrate. The height information allows identifying three different regions with the number of layers marked in the image. (b) Optical near-field image obtained using white light synchrotron radiation. The different layer edges are indicated by black lines. The white square box marks the inset in Fig. 3(b).

To further investigate the optical resolution as well as to compare the strength of the optical response for different materials combinations, linescans inside the optical images are analyzed. In Fig. 3(a) we plot the intensity of the near-field optical signal as a function of the position on the sample along the line marked in the inset. Crossing to areas with different amount of graphene layers, a clear jump in the optical intensity over a distance of ca. 100 nm (optical resolution) is observed. Black lines mark the intensity level for the positions with similar amounts of graphene layers ranging from 0 to more than 4 layers. We marked for every jump the difference in the measured signal. Fig. 3(b) depicts a similar plot for the graphene flake on top of the hBN (the line trace is illustrated in the inset). Again a clear jump is observed between areas with layer numbers indicating the same optical resolution for the two samples. Interestingly, we observe different relative intensity differences for the graphene layers on different surfaces (SiO_2 and hBN).

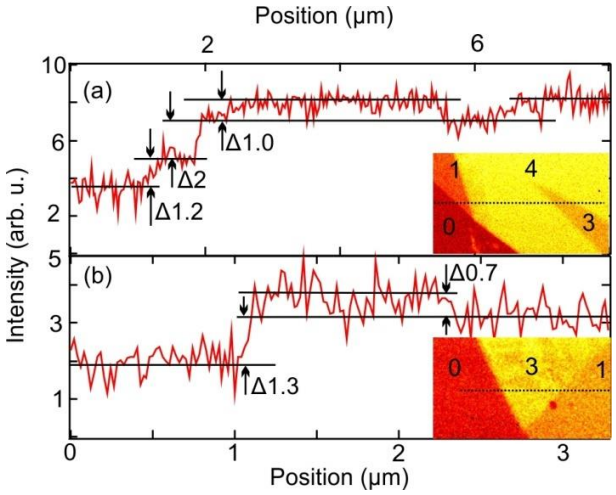

Figure 3: (a) Linescan showing the obtained optical response along the line marked in the inset across different graphene layers onto SiO_2. (b) Linescan showing the optical response along the marked line in the inset of the graphene/hBN sample.

For a better comparison of the optical response for both substrates, we show in Fig. 4 the AFM topography and optical near-field images of another G/hBN heterostructure (hBN flake is ca. 30 nm height) lying on a Si/SiO_2 substrate. We can clearly identify, by their different heights, distinct numbers of graphene layers (1 and 3) lying on hBN and SiO_2. The exact number marked in the image was deduced from Raman spectra. Furthermore, one notices in the AFM image that the graphene layer is not completely flat after the transfer to the hBN flake. Several bubbles and wrinkles, with different heights and shapes, were formed during the transfer process. All different sample regions can be identified by their distinct optical response. The bare hBN and SiO_2 regions exhibit similar optical signal levels, while the G/SiO_2 and G/hBN heterostructures - consisting of 1 layer and 3 layers of graphene - are clearly optically distinguishable. Herby, the G/SiO_2 optical response is much stronger than that of the G/hBN sample.

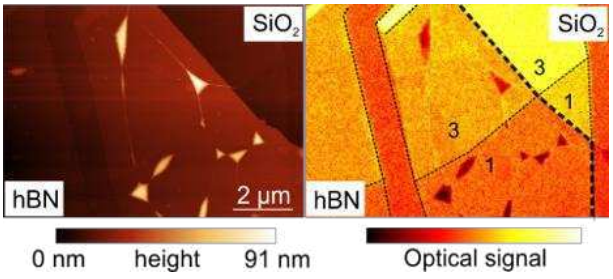

Figure 4: In the left is the AFM image of graphene layers on top of hBN/SiO_2. A graphene flake with 1 and 3 layers extends over the border and touches the underlying SiO_2 substrate. At several positions, the graphene layer formed bubbles and wrinkles. In the

DOI: 10.17648/bwsp-2017-79325

right is the s-SNOM image of the same area. The border of the graphene flake and the border of the hBN are marked by black dotted lines.

Fig. 5(a) shows SINS spectra obtained at different sample positions marked in the inset. Beside this, an SINS spectrum was obtained on the pure SiO_2 surface. In Fig. 5(a) we plot the amplitude of the SINS as function of the wavenumber. For both spectra of the graphene layers, the SiO_2 band is visible. For instance, we observe the typical SiO_2 band[7,12] at ca. 1120 cm^{-1}, and a clear increase of the peak height on the graphene region. Such behavior has been reported before and is ascribed to the interaction of the graphene plasmons with the low frequency lattice vibration of the underlying SiO_2 substrate.[9,13] Furthermore, we see a broad band starting at 800 cm^{-1}, which is cut off by the sensitivity range of our MCT detector. Nevertheless, again this feature has been theoretically predicted[9] and further indicates that we observe the coupling of the graphene plasmon to the low energy phonons of the SiO_2.

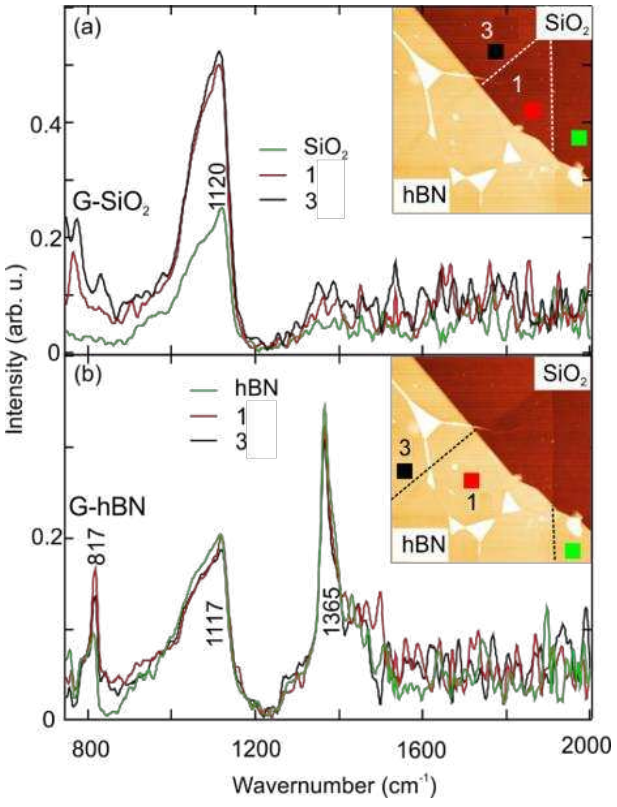

Figure 5: (a) SINS spectra of the G/SiO_2 obtained from the positions marked in the inset. (b) SINS spectra of the G/hBN obtained from positions marked in the inset.

In Fig. 5(b), we depict the mid-IR spectra from 800 cm^{-1} to 2000 cm^{-1} of bare hBN and G/hBN heterostructure. Hexagonal boron nitride is known to show bands in the mid IR far-field spectra at ca. 800 cm^{-1} and 1400 cm^{-1}.[6,7,17] In our SINS spectrum, we observe these two bands at 817 cm^{-1} and 1365 cm^{-1}. Besides these typical bands of hBN, the SiO_2 band at 1130 cm^{-1} is still observed.

Discussion

Overall, the optical response is lower for the graphene on top of hBN substrates, resulting in a higher noise on the optical line traces. Comparing the relative intensity difference between 1 and 3 layers of graphene on a SiO_2 surface, we observe that the signal increases roughly 2 times (1.6x) when changing from the 1 to the 3 layer (normalized to the intensity jump from surface to 1 layer). It increases roughly again 1 time (0.8x), when comparing the 3 layer to the 4 layer. Looking at the same situation for the graphene on the BN surface, a much smaller intensity jump between the single layer and the triple layer is observed (0.5x). In fact, the intensity increases only by half the amount compared to the intensity difference between bare surface and the 1 layer – in the case of a SiO_2 surface the difference is almost 2 times. These results indicate that the optical properties of graphene are influenced by the host surface or substrate. In a first assumption of a metallic state of the graphene, it should behave as a conductive metallic mirror. Then, the expected near-field signal should be proportional to dielectric permeability ϵ.[21] Furthermore, a strong near-field signal is expected from highly conductors materials, as Au or Pt, except in the cases we are exactly at the wavelength of ϵ resonances.[21,25] Therefore, we ascribe the difference in the relative intensity change between layers to a change in the conductivity of the graphene directly influencing ϵ. Such changes in the conductivity have been reported[26] also for transport measurements carried out on graphene deposited on difference surfaces.[22,23,27]

Next, it has been recently shown that the graphene plasmons can couple to the lattice vibrations of hBN in a similar way as they couple to a SiO_2 substrate.[4,6,7,17,18] This plasmon-phonon coupling phenomenon implies the hybridization resonance originating from the surface plasmons modes of the graphene with the modes from substrate lattice, giving rise to the increase of intensity band for lowest energetic phonons.[6,7,17] Therefore, that the strength of the surface plasmons phonon polariton allows the detection of a confinement of phonon–polariton modes in the graphene/hBN heterostructures. Finally, for all spectra of the graphene layers, the SiO_2 and hBN bands are visible. This indicates that the multilayer graphene is too thin to screen the underlying surface from the tip-sample interaction, supporting our

DOI: 10.17648/bwsp-2017-79325

assumption that the graphene mainly acts as dielectric mirror for the mid-IR range. Additionally, shows that 25 nm thick hBN cannot screen the underlying substrate and the penetration depth of the near-field optical signal is not negligible for the dielectric material. Indeed, it has been shown that a single graphene layer is able to extend the penetration depth of the s-SNOM interaction up to 500 nm.[28]

In conclusion, we investigated the near-field optical response of graphene in the mid-IR range using a s-SNOM setup coupled to an IR synchrotron light source. We see a clear difference in the optical signal level from graphene transferred onto different surfaces and we can also observe a strong optical contrast between regions with different numbers of layers in the graphene. Interestingly, we observe a non-linear trend for the optical response as a function of the number of layers. SINS point spectra of the G/SiO_2 and G/hBN heterostructures exhibit a clear signal enhancement for various IR active phonon bands indicating that there is coupling between surface plasmons of graphene and phonons of SiO_2 or the hyperbolic phonon polaritons of hBN. Therefore, our study shows that our setup can systematically image and access the physics of the mid-IR of different combinations of 2D materials with nanoscale resolution.

Acknowledgments

The authors thank Neaspec GmbH for helping to setup the s-SNOM experiment at the IR beamline of the LNLS. A.M and L.C.C acknowledge the financial support from FAPEMIG, Capes, CNPq and INCT-Nanocarbono.

1 Lutz, C. T.; Haven, N.; Physik, T. *IEEE Electron Device Lett.* **2017**, 23 (1).
2 Avouris, P. *Nano Lett.* **2010**, 10, 4285.
3 Bonaccorso, F.; Sun, Z.; Hasan, T.; Ferrari, A. C. *Nat. Photonics* **2010**, 4, 611.
4 Bao, Q.; Loh, K. P. *ACS Nano* **2012**, *6*, 3677.
5 Xia, F.; Wang, H.; Xiao, D.; Dubey, M.; Ramasubramaniam, A. *Nat. Photonics* **2014**, 8, 899.
6 Maia, F. C. B.; O'Callahan, B. T.; Cadore, A. R.; Barcelos, I. D.; Campos, L. C.; Watanabe, K.; Taniguchi, T.; Deneke, C.; Raschke, M. B.; Freitas, R. O. *2017, arXiv:1704.08980* **2017**.
7 Barcelos, I. D.; Cadore, A. R.; Campos, L. C.; Malachias, A.; Watanabe, K.; Taniguchi, T.; Maia, F. C. B.; Freitas, R.; Deneke, C. *Nanoscale* **2015**, 7, 11620.
8 Grasseschi, D.; Bahamon, D. A.; Maia, F. C. B.; Neto, A. H. C.; Freitas, R. O.; de Matos, C. J. S. *2D Mater.* **2017**, 4, 35028.
9 Fei, Z.; Andreev, G. O.; Bao, W.; Zhang, L. M.; S. McLeod, A.; Wang, C.; Stewart, M. K.; Zhao, Z.; Dominguez, G.; Thiemens, M.; Fogler, M. M.; Tauber, M. J.; Castro-Neto, A. H.; Lau, C. N.; Keilmann, F.; Basov, D. N. *Nano Lett.* **2011**, 11, 4701.
10 Chen, J.; Badioli, M.; Alonso-González, P.; Thongrattanasiri, S.; Huth, F.; Osmond, J.; Spasenović, M.; Centeno, A.; Pesquera, A.; Godignon, P.; Zurutuza Elorza, A.; Camara, N.; de Abajo, F. J. G.; Hillenbrand, R.; Koppens, F. H. L. *Nature* **2012**, 487, 77.
11 Dai, S.; Fei, Z.; Ma, Q.; Rodin, A. S.; Wagner, M.; McLeod, A. S.; Liu, M. K.; Gannett, W.; Regan, W.; Watanabe, K.; Taniguchi, T.; Thiemens, M.; Dominguez, G.; Neto, A. H. C.; Zettl, A.; Keilmann, F.; Jarillo-Herrero, P.; Fogler, M. M.; Basov, D. N. *Science,* **2014**, 343, 1125.
12 Fei, Z.; Rodin, A. S.; Andreev, G. O.; Bao, W.; McLeod, A. S.; Wagner, M.; Zhang, L. M.; Zhao, Z.; Thiemens, M.; Dominguez, G.; Fogler, M. M.; Neto, A. H. C.; Lau, C. N.; Keilmann, F.; Basov, D. N. *Nature* **2012**, 487, 82.
13 Wagner, M.; Fei, Z.; McLeod, A. S.; Rodin, A. S.; Bao, W.; Iwinski, E. G.; Zhao, Z.; Goldflam, M.; Liu, M.; Dominguez, G.; Thiemens, M.; Fogler, M. M.; Castro Neto, A. H.; Lau, C. N.; Amarie, S.; Keilmann, F.; Basov, D. N. *Nano Lett.* **2014**, 14, 894.
14 Bechtel, H. A.; Muller, E. A.; Olmon, R. L.; Martin, M. C.; Raschke, M. B. *Proc. Natl. Acad. Sci.* **2014**, 111, 7191.
15 Hermann, P.; Hoehl, A.; Ulrich, G.; Fleischmann, C.; Hermelink, A.; Kästner, B.; Patoka, P.; Hornemann, A.; Beckhoff, B.; Rühl, E.; Ulm, G. *Opt. Express* **2014**, 22, 17948.
16 Hermann, P.; Hoehl, A.; Patoka, P.; Huth, F.; Rühl, E.; Ulm, G. *Opt. Express* **2013**, 21, 2913.
17 Dai, S.; Ma, Q.; Liu, M. K.; Andersen, T.; Fei, Z.; Goldflam, M. D.; Wagner, M.; Watanabe, K.; Taniguchi, T.; Thiemens, M.; Keilmann, F.; Janssen, G. C. A. M.; Zhu, S.-E.; Jarillo-Herrero, P.; Fogler, M. M.; Basov, D. N. *Nat. Nanotechnol.* **2015**, 10, 682.
18 Kumar, A.; Low, T.; Fung, K. H.; Avouris, P.; Fang, N. X. *Nano Lett.* **2015**, 15, 3172.
19 Freitas, R. O.; Maia, F. C. B.; Deneke, C.; Moreno, T.; Dumas, P.; Westfahl, H.; Petroff, Y. *Synchrotron Radiat. News* **2017**, *30* (4), 24–30.
20 Pollard, B.; Maia, F. C. B.; Raschke, M. B.; Freitas, R. O. *Nano Lett.* **2016**, 16, 55.
21 Keilmann, F.; Hillenbrand, R. *Phil. Trans. R. Soc. A* **2004**, 362, 787.
22 Cadore, A. R.; Mania, E.; Watanabe, K.; Taniguchi, T.; Lacerda, R. G.; Campos, L. C. *Appl. Phys. Lett.* **2016**, 108, 233101.
23 Cadore, A. R.; Mania, E.; de Morais, E. A.; Watanabe, K.; Taniguchi, T.; Lacerda, R. G.; Campos, L. C. *Appl. Phys. Lett.* **2016**, 109, 33109.
24 Lafeta, L.; Cadore, A. R.; Mendes-de-Sa, T. G.; Watanabe, K.; Taniguchi, T.; Campos, L. C.; Jorio, A.; Malard, L. M. *Nano Lett.* **2017**, 17, 3447.
25 Anatoly Zayats; David Richards. *Nano-Optics and Near-Field Optical Microscopy*; Artech House: Boston, London, 2008.
26 Abergel, D. S. L.; Russell, A.; Fal'ko, V. I. *Appl. Phys. Lett.* **2007**, 91, 63125.
27 Mania, E.; Alencar, A. B.; Cadore, A. R.; Carvalho, B. R.; Watanabe, K.; Taniguchi, T.; Neves, B. R. A.; Chacham, H.; Campos, L. C. *2D Mater.* **2017**, 4, 31008.
28 Li, P.; Wang, T.; Böckmann, H.; Taubner, T. *Nano Lett.* **2014**, 14, 4400.

DOI: 10.17648/bwsp-2017-79325